Defence Technology 18 (2022) 325–343

Contents lists available at ScienceDirect

Defence Technology

journal homepage: www.keaipublishing.com/en/journals/defence-technology

Performance analysis and design of loitering munitions: A comprehensive technical survey of recent developments

Mark Voskuijl

Faculty of Military Sciences, Netherlands Defence Academy, Den Helder, The Netherlands

ARTICLE INFO

Article history:
Received 7 May 2021
Received in revised form
4 June 2021
Accepted 16 August 2021
Available online 20 August 2021

Keywords:
Loitering munition
Unmanned aerial vehicle
Flight performance
Design

ABSTRACT

Loitering munitions are increasingly used in armed conflicts. An extensive database of loitering munitions is developed based on information available in the public domain. This database includes dimensions, weights, and performance parameters such as flight endurance and communication range. Based upon this dataset, 6 categories of loitering munitions are identified and statistical trends in the form of equations are provided for each category. The statistical trends are supported by aircraft performance theory tailored to loitering munitions applications. Altogether, the combination of the database, statistical trends and aircraft performance theory can be used to analyse the flight performance and design considerations of new loitering munitions of which only limited non-technical information is available in the public domain such as pictures and news articles. Based on the statistical trends and aircraft performance theory it is concluded that for long range applications, the preferred design solution is the conventional configuration. The cruciform configuration is beneficial in case precision flight path control is of prime importance. The tandem wing configuration combines the benefits of a canister launch and relatively high aspect ratio wings suitable for long range flight. Finally, the delta wing design provides a large internal volume and a high terminal attack airspeed. Two example case studies are included to illustrate the flight performance capabilities of two types of loitering munitions used in the current conflict in Yemen (a long range conventional design and a delta wing configuration).

1. Introduction

At a relatively low cost, unmanned aerial systems equipped with a warhead can be used nowadays to target amongst others, tanks, military vehicles and military personnel. This development is rapidly changing the battlefield and allows countries with limited funding and non-state actors to purchase off the shelf air power [1]. Weaponized kamikaze drones have been used with frequent success in the recent Nagorno-Karabakh conflict between Armenia and Azerbaijan. Egozie has appropriately designated this conflict as the first loitering weapon systems war [2]. This development can also be observed in the present conflict in Yemen. Ansar Allah, the Houthi rebel movement has for example used long range unmanned aerial systems in combination with land cruise missiles to target oil refineries in Saudi Arabia [3]. The weaponized kamikaze drones or unmanned aerial systems equipped with a warhead described above are designated in this research article as loitering munitions. These unmanned aerial vehicles are intended to detonate on impact with their target much like a traditional air to ground missile. Consequently, the loitering munitions are not intended for single use and not to be recovered. The definition by the UK Ministry of Defence is used to classify loitering munitions in order to make a clear distinction with cruise missiles, precision guided munitions and unmanned combat aerial vehicles:

> "Loitering munitions are low-cost guided precision munitions that can be maintained in a holding pattern in the air for a certain time and rapidly attack land or sea non-line-of-sight targets. Loitering munitions are under the control of an operator who sees a real-time image of the target and its surrounding area, giving the capacity to control the exact time, attitude, and direction of the attack of a static, relocatable, or moving target, including providing a contribution to the formal target identification and confirmation process" [4].

E-mail address: m.voskuijl@mindef.nl.
Peer review under responsibility of China Ordnance Society

https://doi.org/10.1016/j.dt.2021.08.010

The first loitering munitions such as the Israeli Aerospace Industries Harpy intended for suppression of enemy air defences, were developed in the 1990s. At present however, many different designs are being marketed [5]. The different types of loitering munitions currently used worldwide (listed in Appendix B) can be divided based on their configuration into six main categories:

- Conventional fixed-wing
- Canard
- Delta wing
- Cruciform wing
- Tandem wing
- Rotorcraft

One should realize that in the (near) future other configurations may be developed which would require an extension of this list. Furthermore, designs which fit in multiple categories are also a possibility. For example, one could think of a fixed-wing design with dedicated rotors for a hover and vertical take-off capability.

In terms of the propulsion system, nearly all loitering munitions use propellers or rotors to provide thrust. The power is typically provided by either an electric engine or a gasoline engine. Nearly all fixed-wing designs have a single pusher propeller.

The loitering munitions covered in the present research are used for a variety of targets. They are employed for anti-personnel, anti-armour, anti-structure and suppression of enemy air defences applications. The specific application determines the required type and size of the warhead. Rotary wing loitering munitions are a special category which are used for urban combat. Apart from the type of target, the mission is characterized by the required loitering time (endurance) and the distance of the target (range).

Literature in the engineering sciences on the topic of loitering munitions is primarily focused on guidance, navigation and control aspects including target recognition and swarming techniques. Accurate flight path control under real world conditions such as wind and turbulence is of prime importance for loitering munitions. This topic is addressed by Refs. [6,7]. Besides the ability to follow a prescribed flight path with high accuracy it is also key for mission success to select an effective flight path and to identify ground targets. Optimal path planning strategies for loitering munitions are described in Ref. [8]. Wang et al. [9,10] investigated precise ground target localization using a video camera as sensor for loitering munition applications. On a higher level, collaboration aspects between multiple loitering munitions must be addressed. Research on swarming technologies for loitering munitions can be found in Ref. [11].

A limited number of research articles investigate design aspects of subsystems of loitering munitions or specific vehicles. Liu et al. [12] focus on fuse warhead coordination for loitering munitions. The aerodynamic characteristics of a specific loitering munition design were investigated in Ref. [13]. Research on the aerodynamic design of gun-launched loitering munitions was presented in Ref. [14]. A design method for electric propulsion systems for small loitering munitions is presented in Ref. [15]. A broader perspective on propulsion systems for loitering munitions is provided in Ref. [16].

There appears to be no scientific literature in the field of engineering that addresses overall configuration design and flight performance aspects of loitering munitions. The primary aim of this research article is therefore to provide a comprehensive technical overview of current loitering munitions from a design and aircraft performance perspective. For this purpose, an extensive database of loitering munitions is developed based on information available in the public domain. This database includes dimensions, weights, and performance parameters such as flight endurance and communication range. Configuration design aspects such as the type of propulsion system, the launch method and the planform are also included. Based upon this dataset, statistical trends are provided for different categories of loitering munitions. The statistical trends are supported by aircraft performance theory tailored to loitering munitions applications. Altogether, the combination of a database, statistical trends and aircraft performance theory can be used to analyse the flight performance and design considerations of loitering munitions of which only limited non-technical information is available in the public domain such as pictures and news articles.

This article is structured as follows. In section 2, the relationship between design criteria for loitering munitions and aircraft performance theory is established. A detailed theoretical background of the aircraft performance theory used is given in Appendix A. Sizing correlations and statistical trends are presented in section 3. These sizing correlations are based upon the loitering munitions database which is provided in Appendix B. Two example case studies are presented in Section 4. The first case study addresses the flight performance of a long range fixed-wing loitering munition with a conventional configuration (high aspect ratio wing and conventional empennage) used in the Yemen conflict. The second case study is dedicated to a relatively new loitering munition with a delta wing design. Finally, conclusions and recommendations will be made.

2. Aircraft performance and design criteria

In this section, five high level performance and design criteria are addressed from a theoretical perspective. The total flight time capability of a loitering munition (endurance) is treated first. Next the terminal dive attack airspeed is discussed. The ability to achieve precision control of a trajectory in the presence of external disturbances is the third performance criteria. This ability is also directly related to the inherent controllability of the loitering munition which in turn depends on its configuration. The other two criteria addressed are the ability to perform hovering flight, relevant for urban warfare and the size needed for the launch system. In the final paragraph, a summary is given of the performance and design criteria in relation to the aircraft configuration and its design parameters.

2.1. Loitering endurance

If a flight is conducted at a constant (optimal) angle of attack and a constant altitude, endurance can be calculated with Eqs. (1) and (2). To arrive at these equations it is assumed that the power specific fuel consumption and the propeller efficiency are constant over the range of flight speeds of interest. For a detailed derivation of these equations, the reader is referred to Appendix A.1.

$$E_{\text{piston}} = \frac{\eta_{\text{prop}}}{c_{\text{P}}} \sqrt{\frac{54}{256} \frac{\rho(\pi A e)^3}{C_{D_0}}} \left[\frac{1}{\sqrt{(W/S)_{\text{final}}}} - \frac{1}{\sqrt{(W/S)_{\text{start}}}} \right] \tag{1}$$

$$E_{\text{battery}} = \eta_{\text{elec}} \eta_{\text{prop}} \sqrt{\frac{27}{512} \frac{1}{(W/S)} \frac{1}{W^2} \frac{\rho(\pi A e)^3}{C_{D_0}}} U_{\text{bat}} \tag{2}$$

These equations demonstrate which design parameters are of importance for loitering endurance (E). The propulsion system should have a low power specific fuel consumption (c_{P}) or energy consumption (η_{elec}) and a high propeller efficiency (η_{prop}) at the airspeed at which the aircraft loiters. The aspect ratio (A) and

Ostwald factor (e) are important aerodynamic design parameters. Furthermore, low altitude flights lead to longer endurance. The zero lift drag coefficient (C_{D0}) should be as small as possible. Finally, a low wing loading defined as aircraft weight divided by wing surface area (W/S) and a large fuel fraction (ratio of fuel weight over maximum take-off weight) are design parameters in case of aircraft equipped with internal combustion engines. For electrically powered aircraft the wing loading and the aircraft weight should be as low as possible. A large amount of electric energy (U_{bat}) is evidently also beneficial. However, the energy stored in the batteries has a direct relation to the aircraft weight even though these parameters appear separate in the equation. Some loitering munitions offer the possibility to use either a small or large warhead. With a smaller lightweight warhead, endurance is improved. In short, a conventional aircraft configuration with a long slender wing and a lightweight design is most suitable to achieve good loitering endurance performance. In addition, an efficient propulsion system is needed. Finally, a relatively low airspeed is required during loitering and an appropriate size warhead should be selected.

2.2. Terminal attack dive airspeed

The maximum airspeed (V_{max}) of a loitering munition in a terminal attack dive is defined by Eq. (3).

$$P_{br,max}\eta_{prop}(V_{max}) - C_{D_0}\frac{1}{2}\rho V_{max}^3 S - \frac{2W^2\cos^2\overline{\gamma}}{\pi b^2 e\rho}\frac{1}{V_{max}} + WV_{max}\sin\overline{\gamma} = 0 \quad (3)$$

A derivation of this equation is provided in appendix A.2. The equation is valid for a terminal attack dive at constant airspeed and constant descent angle ($\overline{\gamma}$). Essentially, it consists of four terms; (1) the product of maximum shaft power provided by the engine ($P_{br,max}$) and its propeller efficiency, (2) the power required for zero-lift drag, (3) the power required for lift-induced drag and (4) the time rate of change of the potential energy. The terminal attack dive can be performed at small descent angles or large descent angles. Regardless of the descent angle, a loitering munition designed for a high terminal attack dive airspeed benefits from a high maximum engine shaft power, a propeller pitch angle selected for maximum efficiency at high airspeed (η_{prop}) and a low value of the combined zero lift drag coefficient and wing area ($C_{D_0}S$). The equation is also dependent on the air density (ρ) at the location of the attack.

For shallow descent angles, the time rate of change of potential energy is small and the power required to overcome the zero lift drag is an order of magnitude larger than the power required to overcome the lift induced drag. For steep descent angles, the time rate of change of potential energy becomes an important factor. Hence, it can be concluded that the parameters in the lift-induced drag term have little effect on the maximum airspeed in a terminal attack dive. For significant descent angles it is even helpful to have a large aircraft weight.

2.3. Precision trajectory control

It is of key importance to the design of a loitering munition that the flight trajectory can be controlled precisely, especially in the final phase of the flight. In this phase, atmospheric disturbances such as gusts and turbulence can be encountered. In addition, the target may be moving dynamically.

2.3.1. Atmospheric disturbances

If an aircraft encounter a gust, it will experience an increase in the load factor. As a result it will deviate from its flight path. The load factor increase (Δn) due to a vertical gust with a velocity (U) can be represented with the next equation.

$$\Delta n = K\frac{dC_L}{d\alpha}\frac{\rho UV}{W/S} \quad (4)$$

A derivation of this equation is presented in appendix A.3. Thus, the main design parameters that influence the sensitivity of an aircraft to a gust are the wing loading (W/S) and the lift curve slope ($dC_L/d\alpha$). A high wing loading and a low value of the lift curve slope are beneficial for the gust sensitivity. In addition, operational parameters such as the airspeed and the flight altitude also have an influence. The factor K is related amongst others to the shape of the gust and the length in relation to the vehicle size. The equation demonstrates that the change in load factor due to a gust increases with airspeed. The delta wing configuration is known to have a small lift curve slope compared to other configurations. A delta wing is known to be structurally efficient and provides a large internal volume for a payload. In case the wing loading of a delta wing is similar to other configurations, it is least susceptible to external disturbances.

2.3.2. Agility and controllability

Aircraft with a conventional configuration exhibit what is called non-minimum phase behaviour when changes in the flight path angle are made [17]. When a horizontal flight path is flown, a down force on the tail must be created in order to rotate the aircraft nose-up. Once the aircraft has rotated, the lift will increase and the flight path angle will increase. However, initially the aircraft will have a small downward motion due to the down-force on the tail plane. If the pitch control surface is located ahead of the centre of gravity, such as with the canard configuration, the non-minimum phase behaviour will not be present and the aircraft can respond quicker to control inputs. If primary pitch control surfaces are located close to the centre of gravity, these can be used to directly control the lift force without causing significant rotational motion. Direct lift control allows for an even faster response to desired changes in the flight path angle [18–20]. The cruciform configuration makes it possible to introduce direct a side force control. From a controllability perspective, the cruciform configuration is the preferred solution followed by the canard and tandem configurations. There are significant challenges with respect to the directional stability and control of the delta wing configuration since it does not feature a conventional vertical tail and rudder [21,22]. In some designs vertical tails are added to the wing tips. These tails however have a relatively small moment arm with respect to the centre of gravity and also a relatively small area. Altogether, this leads to a small tail volume. For directional control, drag rudders at the wing tips can be used. This approach has been applied amongst others on the B-2 stealth bomber [22]. Finally, in case different size warheads are possible on a specific design, the selection will impact the weight and balance and thereby the manoeuvrability.

2.4. Size of launch system

There are various methods to launch loitering munitions. The launch method for each loitering munition analysed in the present research is provided in Appendix B.1. The smallest unmanned aerial vehicles which weigh only a few kilograms can be launched by hand. A more common approach is to use a launch rail. Launch rails for small loitering munitions can be carried and set-up manually. In case the loitering munition is large, a mobile launch rail can be

constructed or it can be placed on the back a vehicle or a maritime platform. The disadvantage of using a launch rail is the large volume it requires. If loitering munitions can be folded, they can be stored in what is called a canister. Since these canisters have a relatively small volume, multiple canisters can be placed on a single ground vehicle, maritime platform or even aircraft or helicopter. A small loitering munition stored in a canister can also be carried as a backpack by a soldier. An example is the Hero-30 loitering munition which is stored in a canister from which it is launched by means of a pneumatic system [23]. The capability to transport and launch multiple loitering munitions from a single vehicle is obviously very advantageous from an operational perspective. However, it does have a major impact on the design of the loitering munition since it needs to fit inside a canister. Besides the methods mentioned above, there are some alternative methods to launch loitering munitions. For example, the Burevestnik-MB for example can be stored under the wing of an aircraft [24,25], much like an air to air missile whereas the Defendtex Drone-40 is launched by a grenade launcher [26]. Finally, rotary wing loitering munitions are capable of vertical take-off and landing and do not require a special launch mechanism. Pictures of commonly used approaches are presented in Fig. 1.

2.5. Summary of design criteria

In the previous paragraphs it is explained how aircraft design parameters influence performance criteria relevant for loitering munitions. The relations between design parameters and performance criteria are summarized in Table 1.

It can be observed from Table 1 that various performance criteria are conflicting. A conventional design is likely the best solution if only loitering endurance is considered. However, a conventional configuration with a high aspect ratio wing is difficult to fold into a canister for launch. In case both these requirements are important, an intermediate solution such as a tandem wing may be the best compromise. A design with a canard will also perform well in terms of loitering endurance but probably not as good as a conventional configuration. On the other hand, in terms of manoeuvrability, a canard will outperform a conventional configuration. A delta wing design has a relatively high wing loading and is therefore less susceptible to external disturbances such as gusts when symmetric (longitudinal) motions are considered. Furthermore, the internal volume is relatively large and allows for a large warhead as payload. This in turn, combined with a low wetted area allows for a high terminal attack speed. The directional control of the delta wing configuration remains a significant challenge. The cruciform configuration is especially suitable for precision control. For such a configuration it is a logical design solution to fold the wings. Finally, for special applications such as urban warfare it may be useful to have a design with hover capability. In that scenario a rotorcraft is the preferred configuration. Primary disadvantages of rotorcraft are a low endurance and limited maximum airspeed compared to fixed-wing designs.

There are of course many more aircraft design requirements that play a role in the selection of a configuration for the design of a loitering munition. The discussion above is merely intended to provide insight in the main (conflicting) requirements and possible design solutions. In the next section, sizing correlations of loitering munitions are provided. The observations and conclusions made in the current section will help to understand these sizing correlations.

3. Sizing correlations

An extensive literature study was conducted in order to compare the characteristics of different loitering munitions. This study has resulted in a loitering munitions database which is provided in Appendix B. The database consists of 52 loitering munition designs which are manufactured in 16 different countries. The largest designs can deliver warheads up to 30 kg and have an endurance in the order of 10 h. The smallest designs on the other hand, have a flight endurance of only 10 min and a grenade size warhead. Key performance and design parameters such as endurance, weight and dimensions, are summarized in several figures. The correlations between maximum take-off mass, endurance and warhead mass are presented in Fig. 2, Fig. 3 and Fig. 4 respectively.

It can be observed in Fig. 2 that the preferred configurations for a large warhead mass (in excess of 10 kg) are the conventional-, the delta wing- and the canard configuration. A large warhead mass requires a relatively large aircraft in terms of dimensions and weight. Hence, the requirement for a large warhead mass does not go well with a requirement for a canister launch. These three configurations are inherently not suitable to be folded in a canister. A delta wing design has a relatively large internal volume for a given wing area. This makes it possible to store a large warhead inside. The conventional and canard configuration can have a large wing span and therefore a high aspect ratio. This makes them naturally suitable for long range or high endurance missions. Hence, the same trend is observed in Fig. 3. Furthermore, one can expect that the requirement of a large warhead mass is combined with the requirement for a long endurance.

The sizing correlations in Figs. 2 and 3 include trend lines. These trend lines are defined as power laws as is common in the field of preliminary aircraft design [27,28]. The power laws are obtained by linear regression (least squares fit) of the logarithmic transformation of the data. This approach is described in detail by Verstraete et al. [29] who performed sizing correlations for all types of fixed-wing unmanned aerial vehicles. The power laws can be written as follows (Eq. (5) and Eq. (6)).

Fig. 1. Three examples of common launch methods for loitering munitions. Left: Fire shadow loitering munition launched by rail (image by Think Defence), middle: Hero-30 loitering munition which uses a canister launch method (image by Reise Reise), right: mobile launcher of multiple Chien hsiang loitering munitions (image by Kenchen 945).

Table 1
Summary of performance criteria, design requirements and suitable configurations.

Performance criteria and requirements					
	Loitering endurance	Terminal attack dive speed	Precision trajectory control	Launcher size	Hover capability for urban combat
Relevant design parameters	Low wing loading (W/S) Propeller pitch optimized for cruise flight High aspect ratio (A) wing and large Oswald efficiency factor (e)	Powerful engine ($P_{br,max}$) Propeller pitch optimized for high speed operations Low zero-lift drag and wing area ($C_{D_0}S$) Large aircraft weight (W)	High wing loading (W/S) and small lift curve slope Direct lift control capability Side force control capability Primary control surfaces in front of centre of gravity	Foldable design or small wing span	Rotary wing design
Suitable configurations	Conventional Canard Tandem	Delta wing	Cruciform Canard/Tandem Delta wing (longitudinal control)	Tandem Cruciform Delta wing	Rotorcraft

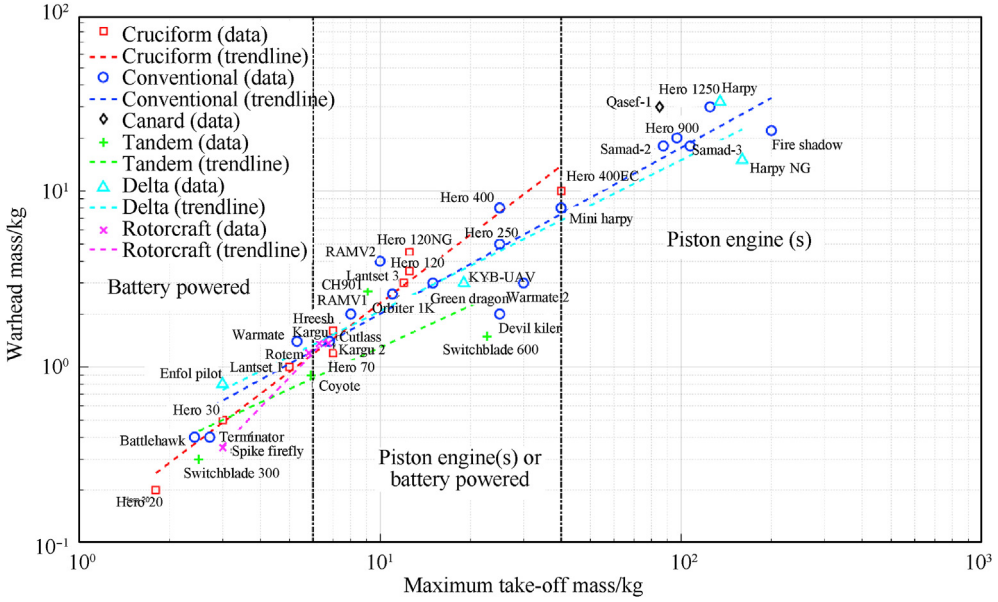

Fig. 2. Relation between warhead mass and maximum take-off mass for different categories of loitering munitions.

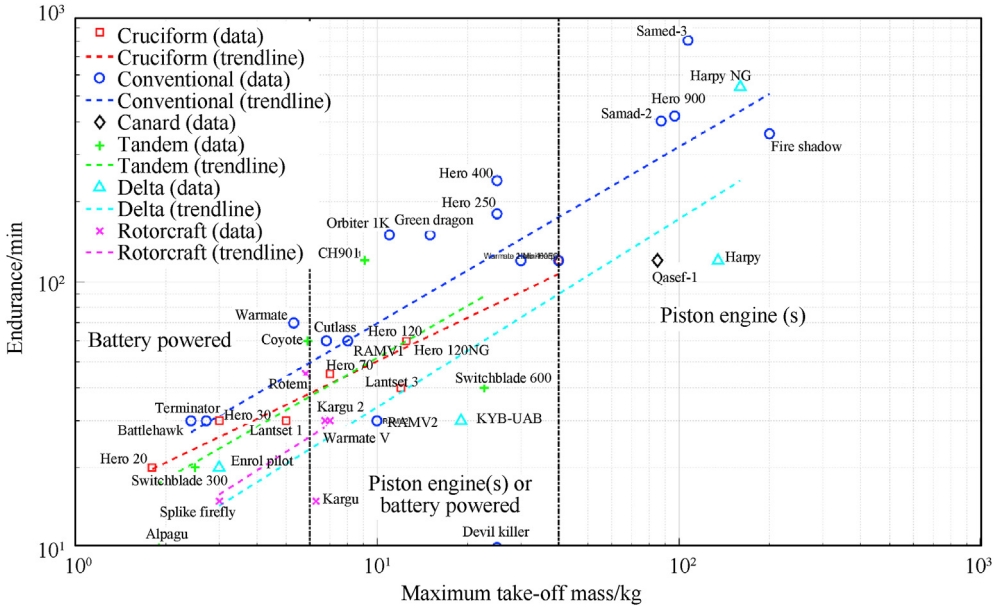

Fig. 3. Relation between endurance and maximum take-off mass for different categories of loitering munitions.

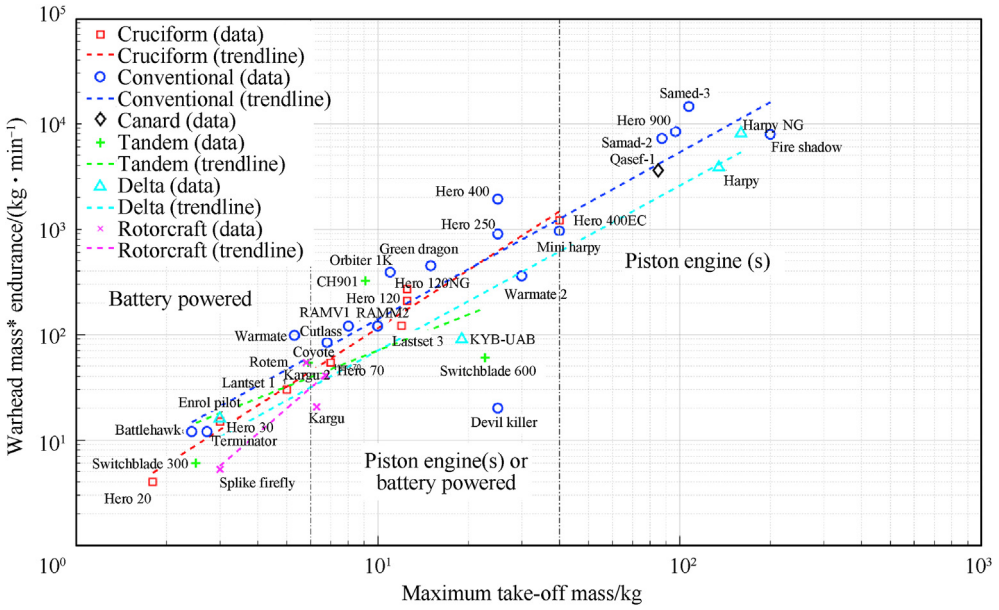

Fig. 4. Product of warhead mass and endurance versus maximum take-off mass for different categories of loitering munitions.

$$m_{\text{warhead}} = B \cdot MTOM^{A} \tag{5}$$

$$\text{endurance} = D \cdot MTOM^{C} \tag{6}$$

The coefficients A, B, C and D in the power laws are provided in Table 2 for each category of loitering munitions. Also included in the table is the number of data points (N) based on which the regression is performed and a measure of the goodness of the linear fit (R^2).

Figs. 2–4 also indicates whether the loitering munitions are powered by batteries and electric motors or gasoline and piston engines. Below 6 kg, all designs have a battery electric propulsion system. The use of a battery-electric propulsion system has an advantage in terms of the acoustic signature (noise). Above a maximum take-off mass of 40 kg, all designs are powered by piston engines. Gasoline has an energy density which is much larger than that of state-of the art Lithium-Ion batteries. On the other hand, the efficiency of electric motors is higher than efficiency of internal combustion engines. This fact does not make up for the difference in energy density. This is why for aircraft with a high endurance, the use of a battery-electric is infeasible. It is expected that these limits will gradually shift over time as the battery energy density increases.

The comparisons in Figs. 2 and 3 are not conclusive because there is a trade-off between payload (warhead mass) and flight range and endurance. To account for this, Fig. 4 presents the product of warhead mass and endurance as a function of maximum take-off mass.

The product of warhead mass and endurance makes it possible to compare the efficiency of different loitering munition configurations. This product is comparable to the well-known product of passengers and flight distance (pax-km) used in civil aviation studies. The trends show clearly that rotorcraft have the lowest efficiency due to their poor aerodynamic efficiency in cruise flight compared to fixed-wing aircraft. But, they have the capability to perform hovering flight which is essential for urban combat. The conventional configuration in general has a high endurance for a given maximum take-off mass due to the efficient aerodynamic design (high aspect ratio wing). The cruciform design is clearly less efficient. There are not sufficient data points for the other configurations (tandem, delta wing and canard) to make firm conclusions with respect to their efficiency. Except for one specific tandem configuration design, the conventional configuration outperforms the tandem, delta wing and canard configurations in terms of efficiency. The trend lines are obtained using the same approach as was done for Figs. 2 and 3. The power law and the corresponding coefficients are provided in Eq. (7) and Table 3.

$$m_{\text{warhead}} \cdot endurance = F \cdot MTOM^{E} \tag{7}$$

In the above discussions, the wing aspect ratio was mentioned several times as an important design parameter to achieve high endurance. The aspect ratio is therefore presented as function of endurance in Fig. 5.

Table 2
Coefficients for the power law correlations of warhead mass and endurance with maximum take-off mass.

Category	Warhead mass correlation with maximum take-off mass				Endurance correlation with maximum take-off mass			
	N	A	B	R^2	N	C	D	R^2
Cruciform	9	1.2945	0.1168	0.9676	8	0.5447	14.3321	0.9187
Conventional	18	0.9422	0.2289	0.9109	17	0.6634	15.1273	0.5427
Canard	1	–	–	–	1	–	–	–
Tandem	4	0.7871	0.2109	0.6002	4	0.6519	11.5213	0.4603
Delta	4	0.8565	0.2892	0.9445	4	0.7076	6.6075	0.7877
Rotorcraft	4	1.7584	0.0514	0.9908	4	0.7228	7.1606	0.2737

Table 3
Correlation of the product of endurance and warhead mass (kg min) with maximum take-off mass.

Category	N	E	F	R^2
Cruciform	8	1.8409	1.6472	0.9803
Conventional	17	1.5831	3.6328	0.7947
Canard	1	–	–	–
Tandem	4	1.1369	5.1238	0.4071
Delta	4	1.5641	1.9111	0.9659
Rotorcraft	4	2.4630	0.3772	0.7836

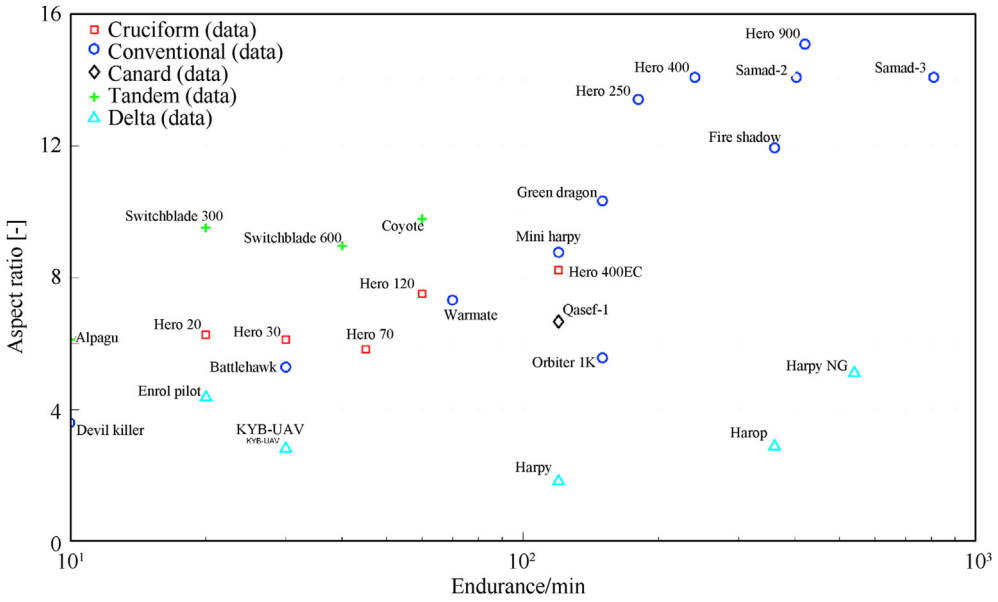

Fig. 5. Wing aspect ratio and endurance for different categories of loitering munitions.

The wing aspect ratio is a key factor with respect to aerodynamic performance (lift over drag ratio) and thereby also with respect to endurance. Other factors such as the detailed aerodynamic shape (fuselage shape, aerofoils, excrescences, etc.) and advanced systems such as active flow control and morphing wings also significantly affect the aerodynamic performance. This explains part of the variations in the data reported in Figs. 1–4. The analysis of loitering munitions reported in this article is however largely based on data obtained in the public domain such as pictures. From these public domain sources it is usually not possible to determine details of the aerodynamic shape and information about the use of advanced systems. An impression of the possible variations in aerodynamic performance for a given wing planform is given by means of an example. It was demonstrated in Ref. [30] that the maximum lift over drag ratio of a tactical unmanned aerial vehicle with a total mass of 50 kg and a conventional wing design with an aspect ratio of 10 could be improved by approximately 16% through the use of aerodynamic shape optimization and active flow control. A second study of the same tactical unmanned aerial vehicle [31] demonstrated the benefits of integrating the flight control system design and morphing wing systems on the flight performance.

Another interesting parameter from a flight performance perspective is the cruise speed. The cruise speed of loitering munitions is often not reported. However, the wing loading is representative for the speed at which the aircraft flies. This follows from the vertical equilibrium equation and the equation for the aerodynamic lift force (Eq. (8)).

$$W = L = C_L \frac{1}{2} \rho V^2 S \tag{8}$$

Hence, the airspeed equation (Eq. (9)) follows:

$$V = \sqrt{\frac{W}{S} \frac{2}{\rho} \frac{1}{C_L}} \tag{9}$$

The lift coefficient (C_L) in cruise flight is typically in the range 0.3–0.6. For a given wing lift coefficient and cruise altitude, the wing loading (W/S) determines the required airspeed. In case the dimensions of an aircraft are increased by a factor n, the wing area will increase with a factor n^2 and the volume increases with a factor n^3. This is called the 'square cube law' and it explains directly why larger aircraft must fly faster than smaller aircraft with the same shape.

The square cube law can be observed in Fig. 6. As maximum take-off mass increases, so does wing loading. In addition, differences between configurations can be seen. The cruciform configuration operates at significantly higher wing loadings and therefore airspeeds than the conventional configuration. Also the tandem configuration typically has a higher wing loading. The wing loading of the conventional configuration is lower because it tends to have a high aspect ratio and a relatively large wing surface area. No clear trend can be seen for the delta wing configuration of which only a limited number of data points are available. Delta wings have a large internal volume for a given wing area. This allows for a large and heavy payload (warhead) which would result in a high wing loading. This seems to be the case for the two delta wing designs with a large maximum take-off mass. The dimensions of the loitering munitions are further analysed in Fig. 7.

The dimensions are of primary importance for the launch method. The majority of loitering munitions is launched by one of the following two methods:

- Canister launch
- Rail launch

If a design can be folded into a canister, the length of the aircraft determines the minimum required length of the canister. The maximum wing span in turn is limited by the length of the canister and the configuration type. Fig. 7 shows that designs with a cruciform configuration have a length more or less equal to the wing span. This means that the full length of the canister is used for the wing assuming that the wing is connected approximately to the middle of the fuselage. In other words, the wing span of cruciform configurations is limited by the canister length. Quite a few designs with a conventional or canard configuration have a wing span larger than the fuselage length. This makes it difficult to fold the design into a container. Such designs are typically launched from a rail. For designs with a tandem configuration, the situation is different. These aircraft have a wing at the front of the fuselage and

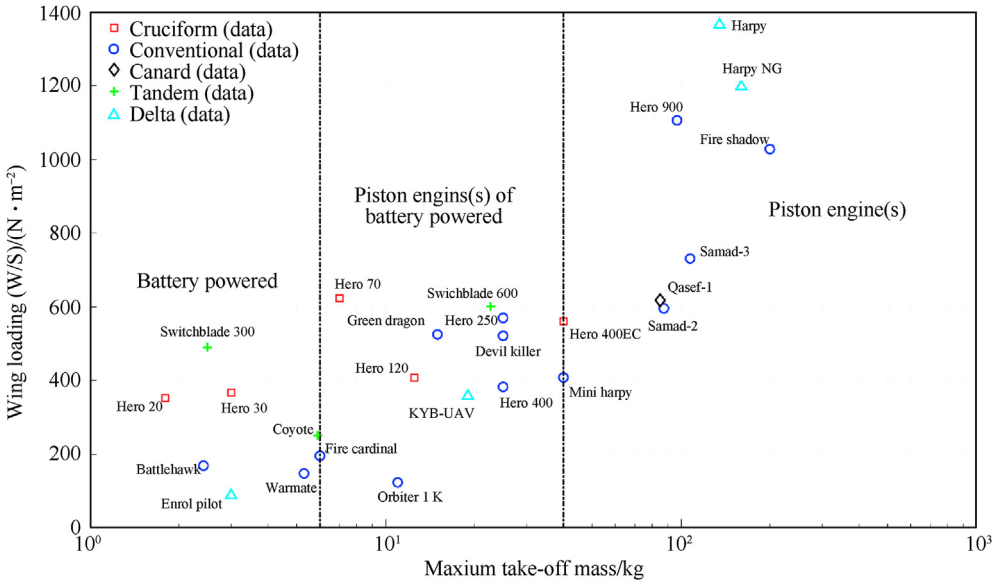

Fig. 6. Wing loading and maximum take-off mass for different categories of loitering munitions.

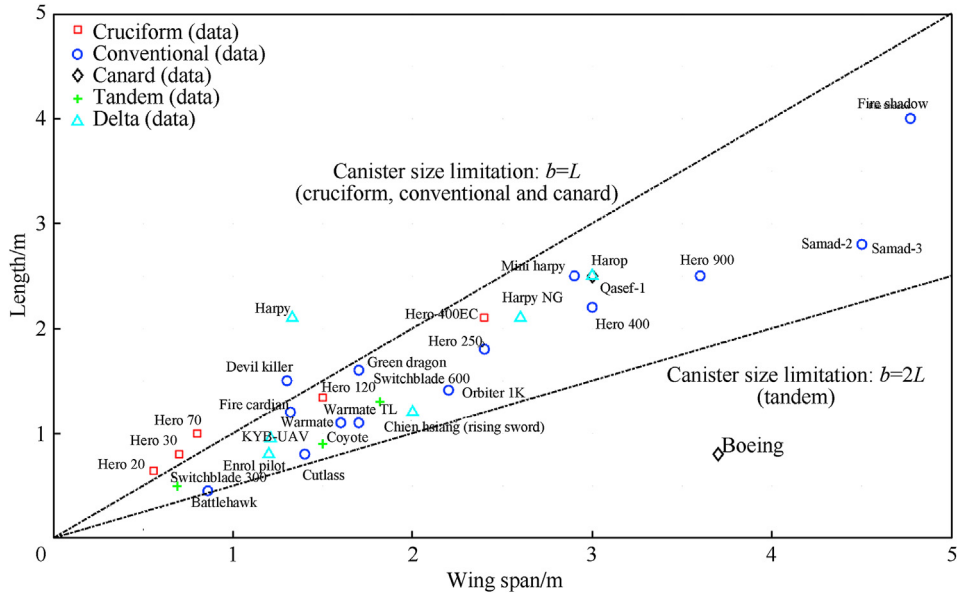

Fig. 7. Wing span and aircraft length for different categories of loitering munitions.

a wing at the rear. This makes it possible to have a wing span twice the length of the fuselage ($b = 2L$) folded into a canister. Hence, the tandem configuration allows for a relatively large aspect ratio whilst satisfying the requirement to be launched from a canister. Finally, delta wing designs cannot be folded easily into a canister. However, for a given wing area and internal volume, the delta wing has a low wing span compared to other configurations. This can be beneficial for the launcher design. The Israel Aerospace Industries (IAI) Harop loitering munition has a special delta wing design. It features wing tips which unfold directly after launch [32]. By doing so, the aerodynamic performance is improved. This vehicle also has a canard configuration which makes it inherently agile.

4. Example case studies

Loitering munitions are frequently used in the conflict in Yemen. Three specific types of loitering munitions used in this conflict are presented as case study in the current section. The flight performance of the Samad 2 and Samad 3 is analysed first. These loitering munitions are designed for long range missions. Next, a loitering munition with a delta wing design is analysed with a focus on its susceptibility to wind gusts.

4.1. Long range conventional configuration – samad 2/3

The Samad loitering munition is operated by Ansar Allah, the Houthi rebel movement. This loitering munition has been used in various long range attacks on targets in Saudi Arabia. Details of

these attacks and the design of this loitering munition are well documented in the yearly reports of the United Nations Panel of Experts on Yemen [3,33]. Based on information available in the public domain, flight performance simulation models of the Samad 2 and Samad 3 loitering munition were developed. These simulation models are largely based on empirical methods to predict the aerodynamic characteristics in terms of lift drag polars [34–40], the propulsion system characteristics in terms of thrust and fuel consumption as a function of airspeed and altitude [41–44] and the mass of the vehicle and the fuel [29]. Mission analyses are performed by means of numerical simulation of the point mass equations of motion. These equations include effects of headwind and crosswind. Two lift drag polars were computed to represent the aerodynamics. The first lift drag polar was constructed based on the DATCOM method [35] in combination with an empirical method (ESDU) to estimate the drag of the antenna of the vehicle [34]. The second lift drag polar was created by estimating the zero lift drag based on handbook methods [36–39] and by estimating the lift induced drag based on a vortex lattice method [40]. The approach to estimate the drag of the antenna was the same as for the first lift drag polar. Results are presented in Fig. 8. Higher fidelity methods to analyse the aerodynamics could not be employed due to a lack of detailed information on the geometry. The uncertainty in the aerodynamic data was accounted for by means of Monte Carlo simulations.

Details of the specific engines used on this aircraft are reported in the earlier mentioned United Nations report [3]. The power specific fuel consumption of these engines are reported by the manufacturer. Less information is known about the propeller. The general dimensions of the propeller were obtained through analysis of a limited number of pictures. The thrust of the propeller was estimated using the parametric ESDU method which relies on a large amount of wind tunnel data of different propellers [41,42]. Finally, estimations were made of the effect of the partial blockage of the propeller by the fuselage [43]. The final static thrust calculated was within 5% of the value suggested by the engine manufacturer in case their recommended propeller was used [45]. Results are presented in Fig. 9.

If more details of the propeller are known, it is possible to determine the propeller thrust as a function of advance ratio by using computational fluid dynamics. Oktay and Eraslan demonstrated that accurate results can be obtained for propellers used on quad rotor unmanned aerial vehicles [46]. All details on the methods used to develop the simulation models of the Samad-2 and Samad-3 are described by Voskuijl et al. [45].

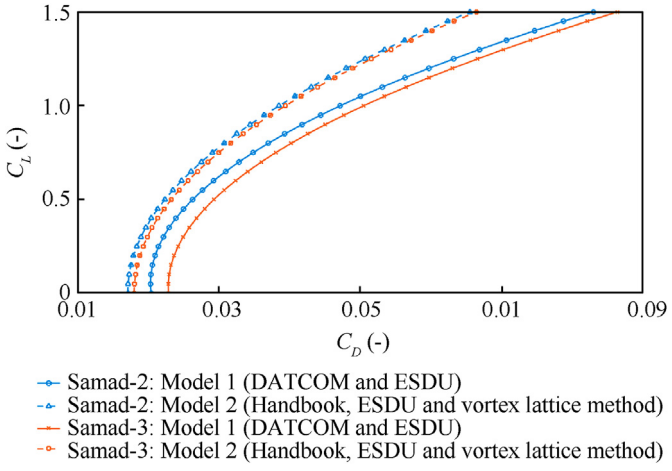

Fig. 8. Lift drag polars of the Samad-2 and Samad-3 at Mach 0.15.

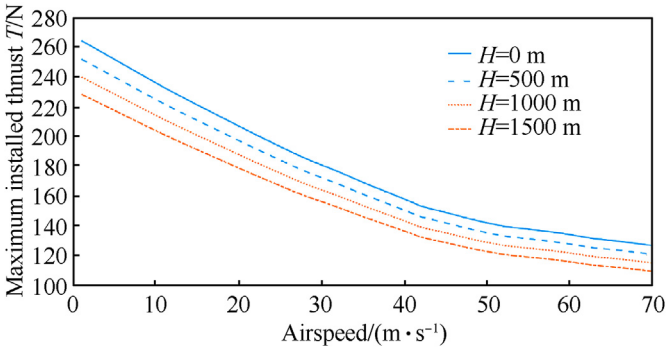

Fig. 9. Maximum installed thrust as a function of airspeed and altitude (ISA condition).

On August 17, 2019 an attack was made with 10 unmanned aerial vehicles on an oil refinery in Shaybah, Saudi Arabia, near the border of the United Arab Emirates. This attack was claimed by the Houthi rebel movement and the United Nations Panel of Experts on Yemen confirmed that the Samad-3 loitering munition was used [3]. In order to give an impression of the flight performance capabilities of the Samad 3 in terms of range, endurance and speed, the simulation model is used to simulate this specific attack on Shaybah. The simulation includes realistic operating conditions including the actual weather conditions (wind, temperature and air density) of the day of the attack. It is assumed that the Samad-3 is launched from a location near Sa'dah in Yemen which is within Houthi controlled territory at a distance of 1234 km from Shaybah. Sa'dah is at a significantly higher elevation than Shaybah. It is further assumed that the loitering munition follows a predefined flight path at 500 m above the terrain and that the best airspeed for maximum range is selected throughout the flight (considering headwind and crosswind effects). The mission is divided into 6 waypoints. The weather conditions at each waypoint are provided in Table 4. These conditions were obtained from a web based application that stores worldwide meteorological data [47]. Some key flight performance parameters throughout the mission are displayed in Fig. 10 (see Table 5).

The baseline flight performance model indicates that the fuel tanks of the Samad-3 are approximately 20% full at the end of the flight. The total fuel volume of the Samad-3 is estimated to be 47.3 L [45]. It should be noted that the simulation model has several uncertainties since it is based on a limited amount of information available in the public domain. A Monte Carlo simulation was therefore conducted to analyse the effect of these uncertainties on the outcome of the simulation. For all possible combinations of uncertainties, the Samad-3 is able to reach Shaybah from Yemen. This confirms that the Samad-3 has long rang capabilities. More details on its range and endurance can be found in Ref. [45].

Other flight performance parameters besides range and endurance are also analysed. The climbing and turning performance of the Samad-2 when operating at its maximum take-off weight and at sea level conditions (international standard atmosphere) is summarized in Fig. 11. This figure is a so-called doghouse chart. The aircraft performance theory required to create this chart is presented in Appendix A.4. The figure displays for the range of achievable airspeeds in steady flight (constant airspeed) which turn rates can be achieved in combination with the achievable climb or descent rate. For example, when the Samad-2 descents with 5 m/s, the maximum airspeed (without turning) is approximately 78 m/s. At the same rate of descent, the aircraft can turn with about 46°/s. In order to achieve that turn rate, the aircraft must fly at approximately 48 m/s. The corresponding turn radius and load factor at this

Table 4
Atmospheric conditions during attack on Shaybah on August 17, 2019 with a Samad-3.

Waypoint	Distance/km	Altitude/m (above mean sea level)	Headwind/(m·s^{-1})	Crosswind/(m·s^{-1})	Air density/(kg·m^{-3})	Temperature/°C
1	0	2379	2.9	0.8	1.0305	33
2	250	1381	2.9	0.8	1.0085	40
3	500	969	3.9	1.0	1.0147	38
4	750	762	8.7	6.7	1.0147	38
5	1000	617	9.5	7.3	1.0210	36
6	1234	585	4.8	3.7	1.0241	35

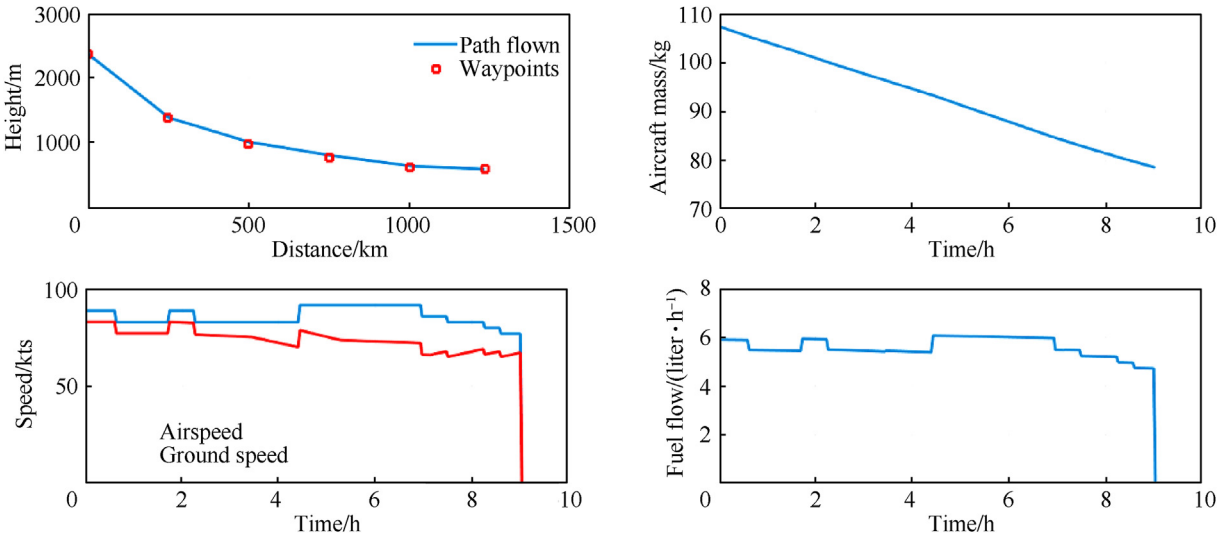

Fig. 10. Simulation of the attack on Shaybah on August 17, 2019 with a Samad-3 under realistic weather conditions.

Table 5
Comparison of sensitivity to wind gusts (flight path accuracy) between the Delta wing UAV and Samad 2/3 loitering munitions.

	Gust sensitivity parameter: $\frac{dC_L}{d\alpha}\frac{1}{W/S}$ (see Eq. (4))	
	Minimum estimate	Maximum estimate
Delta wing UAV	0.0046	0.0070
Samad-2	0.0077 (+67%)	0.0104 (+50%)
Samad-3	0.0065 (+41%)	0.0082 (+17%)

condition are 60 m and 4 g respectively. It should be noted that the performance of this airplane improves significantly when it is operating at a lower weight (for example at the final flight stage when most fuel is burnt).

4.2. Delta wing UAV

Since 2019, it is reported that Houthi rebels in Yemen have been using a new type of loitering munition with a delta wing configuration for several attacks [3]. Examples are the attacks on Saudi Arabian oil pumping stations in Dawadimi and Afif and the well-known attack on the oil installations of Abqaiq on September 14, 2019. This vehicle carries a warhead of 18 kg which is stored in the nose cone and appears to be designed to penetrate heavy armour [3,33]. The dimensions of the Delta wing UAV are reconstructed based on the analysis of several pictures of debris available in the public domain (see Fig. 12). The estimated dimensions are in close agreement with the wing span and vehicle length reported by the Panel of Experts on Yemen [3]. It has a wing surface area (excluding

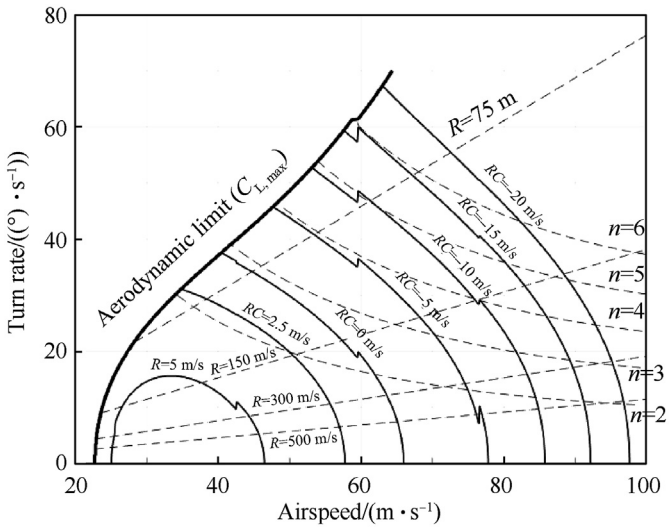

Fig. 11. Doghouse chart of the Samad-2 at sea level conditions (international standard atmosphere) and maximum take-off weight.

the winglets) of 2.17 m^2 and a high main wing leading edge sweep angle of 53°. Altogether this results in a low aspect ratio ($A \approx 1.95$) configuration. The vehicle is powered by a 28 kW Wankel engine with a single propeller. This engine has a very high power to weight ratio.

An analysis of the aerodynamic characteristics of the delta wing UAV was conducted. A vortex lattice method with a leading edge

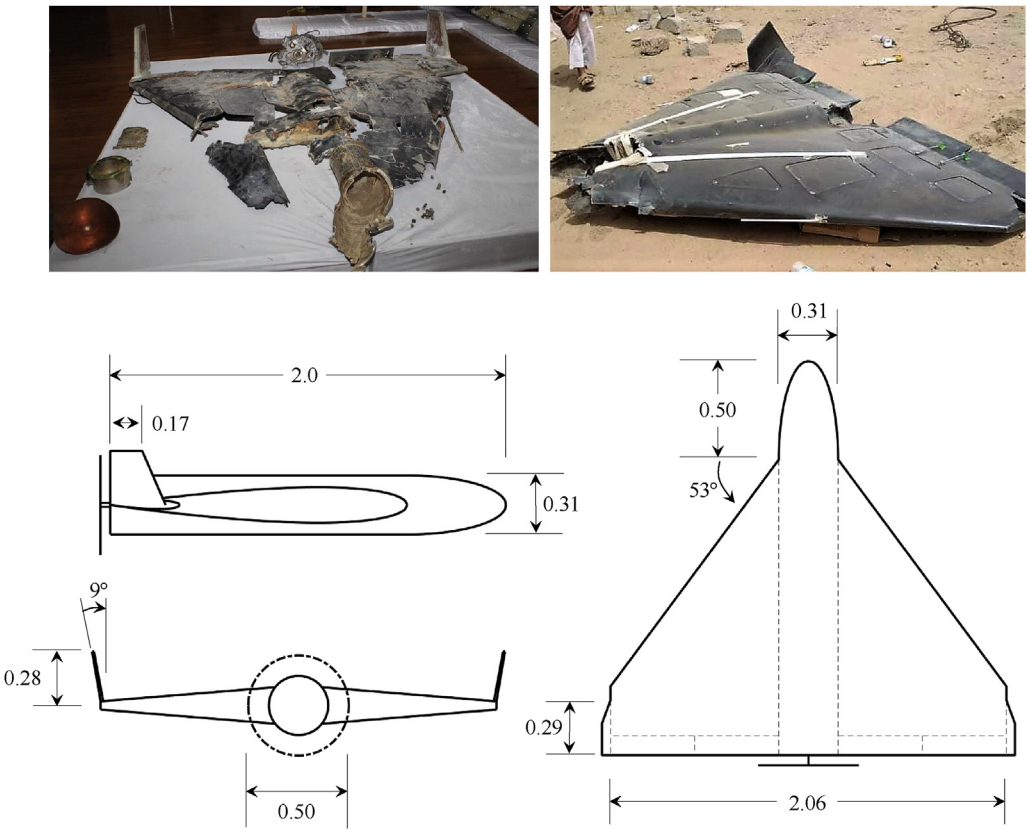

Fig. 12. Debris of delta wing UAV (sources [3,48]) and three view drawing (dimensions in meters) based on analysis of various pictures available in the public domain.

suction analogy was used to predict the lift and induced drag [49–52]. This method is particularly suitable for the analysis of low aspect ratio designs. It is unfortunately not possible to use higher fidelity methods without more detailed knowledge of the aerofoils used in the design. The aerodynamic analysis is extended with a flat plate theory [36] to estimate the zero lift drag coefficient. Results of the analysis indicate that the value of the lift curve slope $dC_L/d\alpha$ equals 2.60 [rad^{-1}]. The lift curve slopes of the Samad 2 and 3 are predicted within the range of 5.92–5.99 by different aerodynamic analysis method. The estimated lift curves of both the Samad and Delta wing UAVs are presented in Fig. 13 for angles of attack up to 10° (within the linear regime).

The maximum take-off mass of the delta wing UAV can be estimated based on aircraft design sizing correlations. Verstraete [29] has reported sizing correlations for unmanned aircraft. These

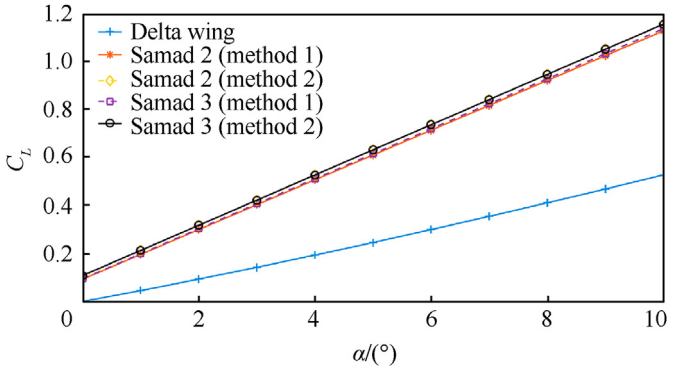

Fig. 13. Estimates of the lift curves of the Samad-2, Samad-3 and Delta wing UAV.

relations predict a maximum take-off mass of 82 kg. However, these correlations are largely based on designs with a higher aspect ratio and are possibly on the low end. Based on the correlations presented in Fig. 2 and Table 2, one would rather expect a maximum take-off mass of 124 kg. Based on the range of mass estimates, the wing surface area and the lift curve slope, a comparison between the sensitivity to wind gusts can be made (Eq. (4)).

The comparison indicates that the conventional design of the Samad 2 and 3 which have the same payload weight as the delta wing UAV (warhead of 18 kg) is significantly more susceptible to wind gusts than the delta wing UAV. Hence, precision flight path control in realistic operating conditions is easier with the delta wing UAV when symmetric flight is considered. The directional stability and control of a delta wing configuration is a significant challenge [22]. In addition, the delta wing UAV has a much smaller wing span compared to the Samad 2 and 3 (2.06 m versus 4.5 m) which is beneficial for the launcher design. Finally, the delta wing UAV has an engine which delivers about twice as much shaft power than the engine installed on the Samad 2 and 3. Considering the fact that the wetted surface area of the delta wing UAV is less than the Samad 2 and 3, it will have a significantly higher maximum airspeed. Altogether, the analysis described highlights the advantages and disadvantages of a loitering munition with a delta wing design compared to a loitering munition with a conventional design from an aircraft performance perspective.

5. Conclusions and recommendations

A comprehensive database of 52 loitering munitions developed in 16 countries was developed based on data available in the public domain. The database includes information on the maximum take-

off mass, warhead mass, dimensions, and flight endurance and communication range. In addition, the launch methods and vehicle configurations are reported. Based on a statistical analysis of the database in combination with aircraft performance theory tailored to loitering munitions several conclusions can be drawn. Six main configurations can be identified; (1) conventional, (2) delta wing, (3) tandem wing, (4) canard, (5) cruciform, and (6) rotorcraft. Loitering munitions can also be categorized based on their propulsion system (battery electric or gasoline powered) or launch method (hand launched, rail launched and canister). For long range applications, the preferred design solution is the conventional configuration. The maximum vehicle mass and warhead mass are 200 kg and 32 kg respectively. The maximum reported endurance is 9 h and flight ranges in excess of 1500 km are estimated for some vehicles. For urban combat, rotary wing vehicles are used because of their vertical flight capability. These vehicles can typically carry grenade size warheads. The cruciform configuration is beneficial in case precision flight path control is of prime importance. The tandem wing configuration combines the benefits of a canister launch and relatively high aspect ratio wings suitable for long range flight. The delta wing design provides a large internal volume and a high terminal attack airspeed.

The statistical trends are presented in various graphs and regression analyses are performed to obtain the relations between warhead mass, endurance and maximum take-off mass for each loitering munition configuration. Based on these trends, performance estimations can be made of vehicles of which only general dimensions are known. For example dimensions based on pictures in the public domain.

Two case studies of vehicles used currently in the conflict in Yemen are reported. A simulation of the Samad 3 loitering munition demonstrates that the attacks on an oil refinery in Shaybah, Saudi Arabia (August 17, 2019) could have been launched from Houthi territory in Yemen (>1200 km range). This illustrates the long range capabilities of loitering munitions with a conventional configuration. The second case study investigates a new delta wing design used by Ansar Allah, the Houthi rebel movement in Yemen. Compared to the Samad 2 and 3, this delta wing loitering munition is much less susceptible to atmospheric disturbances (beneficial for precision flight path control), it has a large internal volume to store a warhead and other systems and it has a much smaller wing span (beneficial for launcher size).

It is recommended to continuously update the loitering munitions database once new developments and designs are reported. Second, it is recommended for future research to perform high fidelity simulations of selected designs once more detail becomes available about their respective geometries (for example air foils used) and structural designs. Such high fidelity simulations can be used for verification and validation purposes. A third recommendation is to perform a quantitative analysis of the flight path precision capability of an attack expressed in a parameter such as the circular error probable for different configurations such as the cruciform design.

Declaration of competing interest

The authors declare that they have no known competing financial interests or personal relationships that could have appeared to influence the work reported in this paper.

Acknowledgements

This research did not receive any specific grant from funding agencies in the public, commercial, or not-for-profit sectors.

Appendix A. Aircraft Performance

A.1 Loitering endurance

The loitering endurance (E) is defined as the total flight time in cruise flight. In this appendix, Eqs. (1) and (2) for loitering endurance of both gasoline and battery-electric unmanned aircraft are derived. Fuel or electric energy is also required for other mission phases such as take-off, climb and descent. These mission phases are not included in the analysis since the main purpose is to determine which design parameters have the largest influence on the loitering endurance. Endurance is the integral of the total time (t) from the start of the cruise phase until the end of the cruise phase (Eq. (A.1)).

$$E = \int_{t_{start}}^{t_{final}} \mathrm{d}t \tag{A.1}$$

In order to calculate this integral it is necessary to determine the required power for cruise flight and the associated fuel flow in case of an internal combustion engine or the consumption of the energy stored in the batteries in case of an electrically powered aircraft. The cruise flight of the aircraft can be assumed quasi-steady since altitude and flight speed (V) will only change gradually. Hence, the following equilibrium equations (Eq. (A.2) and Eq. (A.3)) apply.

$$L = W = C_L \frac{1}{2}\rho V^2 S \tag{A.2}$$

$$T = D = C_D \frac{1}{2}\rho V^2 S \tag{A.3}$$

where C_L and C_D are the dimensionless lift and drag coefficients. These coefficients depend on the shape of the aircraft, the angle of the vehicle with respect to the airflow and the Mach and Reynolds numbers. L and D are the aerodynamic lift and drag force respectively. T represents the thrust provided by the propulsion system. The power required (P_r) for cruise flight is the drag force multiplied with the airspeed (Eq. (A.4)).

$$P_r = \sqrt{\frac{W^3}{S}\frac{2}{\rho}\frac{C_D^2}{C_L^3}} \tag{A.4}$$

In case of aircraft with an internal combustion engine, the time can be related to the fuel flow (F) as defined in Eq. (A.5) and the fuel flow is related to the shaft power (Eq. (A.6)).

$$F = -\frac{\mathrm{d}W}{\mathrm{d}t} \tag{A.5}$$

$$F = c_P P_{br} \tag{A.6}$$

The shaft power (P_{br}) is converted into power available (P_a) for flight by means of the propeller (Eq. (A.7)).

$$P_a = \eta_{prop} P_{br} \tag{A.7}$$

In this equation, η_{prop} represents the propeller efficiency. For electrically powered aircraft, the shaft power depends on the time rate of change of the energy stored in the batteries and the efficiency of the conversion into mechanical power (η_{elec}) (see Eq. (A.8)).

$$P_{br} = -\eta_{elec}\frac{\mathrm{d}U_{bat}}{\mathrm{d}t} \tag{A.8}$$

Combining equations A.1 and A.4-A.8 yields an equation for the endurance of aircraft powered by a piston engine (Eq. (A.9)) and an equation for the endurance of an electric aircraft powered by batteries (Eq. (A.10)).

$$E_{\text{piston}} = \int_{W_{\text{final}}}^{W_{\text{start}}} \frac{\eta_{\text{prop}}}{c_{\text{P}}} \sqrt{\frac{S}{W}\frac{\rho}{2}\frac{C_{\text{L}}^3}{C_{\text{D}}^2}}\,\text{d}W \tag{A.9}$$

$$E_{\text{battery}} = \int_{U_{\text{bat,final}}}^{U_{\text{bat,start}}} \eta_{\text{elec}}\eta_{\text{prop}} \sqrt{\frac{S}{W}\frac{\rho}{2}\frac{C_{\text{L}}^3}{C_{\text{D}}^2}}\,\text{d}U_{\text{bat}} \tag{A.10}$$

It is assumed that the efficiencies and the power specific fuel consumption are constant for the range of flight speeds and flight altitudes of interest. In case a cruise flight is conducted at constant altitude and constant angle of attack, then the air density, the lift coefficient and the drag coefficient are all constant. For this specific flying strategy, the endurance integrals can be solved (see Eq. (A.11) and Eq. (A.12)).

$$E_{\text{piston}} = \frac{\eta_{\text{prop}}}{c_P} \sqrt{\frac{S\rho}{2}\frac{C_{\text{L}}^3}{C_{\text{D}}^2}} \left[\frac{2}{\sqrt{W_{\text{start}}}} - \frac{2}{\sqrt{W_{\text{final}}}}\right] \tag{A.11}$$

$$E_{\text{battery}} = \eta_{\text{prop}}\eta_{\text{elec}} \sqrt{\frac{S}{W^3}\frac{\rho}{2}\frac{C_{\text{L}}^3}{C_{\text{D}}^2}} U_{\text{bat}} \tag{A.12}$$

The lift drag polar describes the relation between the lift coefficient and the drag coefficient. A two term lift drag polar is used in this derivation (Eq. (A.13)).

$$C_{\text{D}} = C_{\text{D}_0} + \frac{C_L^2}{\pi Ae} \tag{A.13}$$

In real life applications it is more accurate to use a three term lift drag polar [53]. However, this derivation is primarily intended to obtain more insight in the physics of the problem and the influence of aircraft design parameters on endurance. In case a two term lift drag polar is used, the optimal ratio of lift coefficient and drag coefficient for maximum endurance can be determined as presented in Eq. (A.14), Eq. (A.15) and Eq. (A.16).

$$\frac{\text{d}}{\text{d}C_{\text{L}}}\left(\frac{C_{\text{L}}^3}{C_{\text{D}}^2}\right) = 0 \tag{A.14}$$

$$C_{\text{L}} = \sqrt{3C_{\text{D}_0}\pi Ae} \tag{A.15}$$

$$C_{\text{D}} = 4C_{\text{D}_0} \tag{A.16}$$

Based on this result the final loitering endurance equations (Eq. (A.17) and Eq. (A.18)) can be determined.

$$E_{\text{piston}} = \frac{\eta_{\text{prop}}}{c_{\text{P}}} \sqrt{\frac{54}{256}\frac{\rho(\pi Ae)^3}{C_{\text{D}_0}}} \left[\frac{1}{\sqrt{(W/S)_{\text{final}}}} - \frac{1}{\sqrt{(W/S)_{\text{start}}}}\right] \tag{A.17}$$

$$E_{\text{battery}} = \eta_{\text{elec}}\eta_{\text{prop}} \sqrt{\frac{27}{512}\frac{1}{(W/S)}\frac{1}{W^2}\frac{\rho(\pi Ae)^3}{C_{\text{D}_0}}} U_{\text{bat}} \tag{A.18}$$

A.2 Terminal attack dive airspeed

A schematic representation of the forces acting on a loitering munition in a powered descending flight at constant airspeed (V) and descent angle ($\overline{\gamma}$) is provided in Fig. A1. The lift vector is by definition perpendicular to the airspeed vector and the aerodynamic drag is parallel to the airspeed vector in opposite direction. The thrust vector is assumed to be aligned with the nose of the aircraft. Since the airspeed and descent angle are constant, all accelerations are zero.

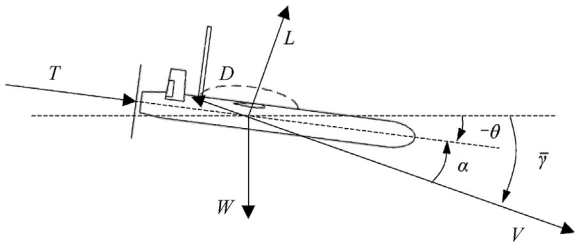

Fig. A1. Descending flight at constant airspeed and descent angle.

The angle θ is the attitude of the aircraft relative to the horizon. The angle of attack (α) is the angle between the airflow and the aircraft. Based on this schematic, the point mass equations of motion can be derived for a powered steady rectilinear descending flight (Eq. (A.19) and Eq. (A.20)).

$$0 = T\cos\alpha_{\text{T}} - D + W\sin\overline{\gamma} \tag{A.19}$$

$$0 = L - W\cos\overline{\gamma} + T\sin\alpha_{\text{T}} \tag{A.20}$$

Eq. (A.2) shows that at the maximum airspeed, the lift coefficient (C_{L}) will be small and therefore the angle of attack as well. Assuming that the thrust force is in line with the nose of the aircraft, the thrust angle of attack α_T will be close to zero. The effect of the thrust angle of attack on the maximum airspeed can therefore be neglected. Equations A.3 and A.4 representing the lift and drag force can be inserted in these equations of motion. By doing so, the airspeed appears as a variable. Furthermore, when Eq. (A.19) is multiplied with the airspeed, the so-called power equation is obtained (Eq. (A.21)).

$$0 = P_{\text{a}} - C_{\text{D}}\frac{1}{2}\rho V^3 S + WV\sin\overline{\gamma} \tag{A.21}$$

To maintain equilibrium perpendicular to the flight path, Eq.

(A.22) must be satisfied.

$$C_L = \frac{2W\cos\overline{\gamma}}{\rho V^2 S} \tag{A.22}$$

By combining equations A.21, A.22 and the equation representing the lift drag polar (Eq. (A.13)) the following relation (Eq. (A.23)) is found:

$$0 = P_a - C_{D_0}\frac{1}{2}\rho V^3 S + \frac{2W^2\cos^2\overline{\gamma}}{\pi b^2 e\rho}\frac{1}{V} + WV\sin\overline{\gamma} \tag{A.23}$$

In order to achieve the maximum airspeed, maximum shaft power should be provided by the propulsion system (Eq. (A.7)).

$$0 = P_{br,max}\eta_{prop}(V_{max}) - C_{D_0}\frac{1}{2}\rho V_{max}^3 S + \frac{2W^2\cos^2\overline{\gamma}}{\pi b^2 e\rho}\frac{1}{V_{max}} + WV_{max}\sin\overline{\gamma} \tag{A.24}$$

When the characteristics of the aircraft are known and the descent angle is defined, Eq. (A.24) can be solved for the airspeed.

A.3 Sensitivity to gusts

If an aircraft encounters a vertical gust in horizontal flight, the angle of attack will change. As a consequence the lift will change and the aircraft will acquire an acceleration perpendicular to its flight path. The load factor (n), defined as the lift divided by the aircraft weight is directly related to this acceleration. The encounter of a gust is presented in Fig. A2.

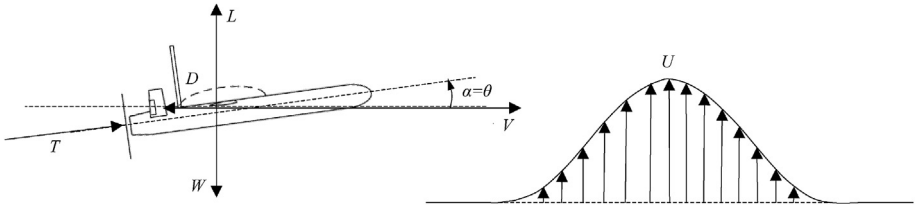

Fig. A2. Vertical gust encounter.

Assuming the aircraft encounters a sharp edged gust, the instantaneous change in the lift coefficient can be written as follows (Eq. (A.25)):

$$\Delta L = \frac{dC_L}{d\alpha}\Delta\alpha\frac{1}{2}\rho\left(V^2 + U^2\right)S \tag{A.25}$$

It is further assumed that the slope of the lift curve is linear. The change in angle of attack ($\Delta\alpha$) is related to the gust velocity (U) and the airspeed (V) of the aircraft (Eq. (A.26)).

$$\Delta\alpha = \tan^{-1}\frac{U}{V} \tag{A.26}$$

An approximation of the instantaneous change in load factor follows (Eq. (A.27)) by combining Eq. (A.24) and Eq. (A.25) and by assuming that the airspeed is significantly larger than the gust velocity.

$$\Delta n = \frac{dC_L}{d\alpha}\frac{\rho UV}{W/S} \tag{A.27}$$

In reality, the gust will not be sharp edged. Furthermore, depending on the size of the aircraft in relation to the gust length, the wing may experience the gust at a different time than the horizontal tail plane or canard. To account for these factors, Eq. (A.26) may be multiplied with a parameter K. More details on this factor are provided by Hoblit [54].

A.4 Doghouse charts

A doghouse chart summarizes the turning and climbing/descending performance of an aircraft for a given flight altitude and thrust setting. This chart is based on the point mass equations of motion for a steady non-sideslipping banked turn [44] (see Eq. (A.28), Eq. (A.29) and Eq. (A.30)):

$$T\cos\alpha_T - D - W\sin\gamma = 0 \tag{A.28}$$

$$W\cos\gamma\sin\mu - \frac{W}{g}\frac{V^2}{R}\cos^2\gamma\cos\mu = 0 \tag{A.29}$$

$$-T\sin\alpha_T - L + W\cos\gamma\cos\mu - \frac{W}{g}\frac{V^2}{R}\cos^2\gamma\sin\mu = 0 \tag{A.30}$$

where μ represents the aerodynamic angle of roll. The turn radius (R) and turn rate ($\dot{\chi}$) are related through the airspeed (Eq. (A.31)).

$$V = \dot{\chi}R \tag{A.31}$$

To achieve the best turning performance, maximum thrust should be applied. Lift, drag in the equations above are a function of the airspeed, the air density and the lift coefficient and drag coefficients. The relation between the lift coefficient and drag coefficient is determined by the lift-drag polar. The angle of attack follows from the lift curve slope if the lift coefficient is known. Based on the inclination of the thrust vector with respect to the aircraft body axis, the thrust angle of attack can be computed.

If the thrust (T) is set at its maximum value and the aerodynamic characteristics of an aircraft are known, then for a given airspeed (V), air density (ρ) and turn rate ($\dot{\chi}$), the point mass equations of motion can be solved iteratively in order to find the required lift coefficient (C_L), flight path angle (γ) and aerodynamic angle of roll (μ). The rate of climb or descent associated to a specific turn rate and air speed follows from Eq. (A.32).

$$\dot{h} = V\sin\gamma \tag{A.32}$$

Appendix B. Loitering weapon systems database

Table B1
Loitering weapon systems general characteristics

Manufacturer	Name	Configuration	Launch method	Propulsion	Engine	Ref.
Armenia						
ProMAQ	Hreesh	Cruciform	Canister	1 propeller		[55]
Australia						
Defendtex	Drone-40	Rotorcraft	Grenade launcher	4 rotors	Electric	[26]
Belarus						
Scientific-Manufacturing Centre of Multipurpose Unmanned Systems	Burevestnik MB	Delta wing	In-flight (under wing)	1 propeller	Piston	[24,25]
China						
China Aerospace Science and Technology Corporation	CH-901	Tandem	Canister	1 propeller	Electric	[56–58]
Europe						
MDBA Missile Systems	Fire Shadow	Conventional	Launcher	1 propeller	Piston	[4,5,59,60]
Indonesia						
PT Enrol Sistem	Enrol Pilot	Delta wing	Hand	1 propeller	Electric	[61]
Iran						
Iran Aircraft Manufacturing Industrial Company (HESA)	Qasef-1/Ababil-2t	Canard	Launcher	1 propeller	Piston	[56,62–65]
Iran Aircraft Manufacturing Industrial Company (HESA)	Qasef-2K*	Canard	Launcher	1 propeller	Piston	[3,65]
Israel						
Aeronautics	Orbiter 1 K	Conventional	Launcher	1 propeller	Electric	[2,66–68]
Elbit Systems	Skystriker	Conventional	Launcher	1 propeller	Electric	[69,70]
IAI	Green Dragon	Conventional	Canister	1 propeller	Electric	[2,71,72]
IAI	Harop	Delta wing	Launcher	1 propeller	Piston	[2,5,56,73,74]
IAI	Harpy	Delta wing	Launcher	1 propeller	Piston	[5,74–77]
IAI	Harpy NG	Delta wing	Launcher	1 propeller	Piston	[4,5,74,76,78]
IAI	Mini Harpy	Conventional	Canister	1 propeller	Electric	[79]
IAI	Rotem	Rotorcraft	VTOL	4 rotors	Electric	[2,71]
Rafael Advanced Defence Systems	Spike Firefly	Rotorcraft	VTOL	2 rotors	Electric	[80]
Poland						
WB Electronics	Warmate	Conventional	Launcher	1 propeller	Electric	[4,67,81,82]
WB Electronics	Warmate 2	Conventional	Launcher	1 propeller	Electric	[83]
WB Electronics	Warmate TL	Conventional	Canister	1 propeller	Electric	[83]
WB Electronics	Warmate V	Rotorcraft	VTOL	6 rotors	Electric	[84]
Russia						
Zala Aero Group	KYB-UAV	Delta wing	Launcher	1 propeller	Electric	[85,86]
Zala Aero Group	Lantset 1	Cruciform		1 propeller	Electric	[86]
Zala Aero Group	Lantset 3	Cruciform		1 propeller	Electric	[86]
South Korea						
Korean Aerospace Industries	Devil Killer	Conventional			Electric	[5,87–89]

(*continued on next page*)

Table B1 (*continued*)

Manufacturer	Name	Configuration	Launch method	Propulsion	Engine	Ref.
				2 propellers		
Turkey						
STM	Alpagu	Tandem	Canister	1 propeller	Electric	[90]
STM	Kargu	Rotorcraft	VTOL	4 rotors	Electric	[90]
STM	Kargu-2	Rotorcraft	VTOL	4 rotors	Electric	[91]
Ukraine						
CDET	RAM	Conventional		1 propeller	Electric	[92]
United States						
AeroVironment	Switchblade 300	Tandem	Canister	1 propeller	Electric	[4,93,94]
AeroVironment	Switchblade 600	Tandem	Canister	1 propeller	Electric	[93–95]
Boeing	Persistent Munition Technology Demonstrator	Canard	Landing gear	1 propeller	Piston	[5,96]
L3 Technologies	Cutlass	Conventional	Canister	1 propeller	Electric	[5,97]
Lockheed Martin Missiles and Fire Control	Terminator	Conventional	Hand	2 propellers	Electric	[4,98,99]
Lockheed Martin Missiles and Fire Control	Terminator (new version)	Conventional	Canister	1 propeller	Electric	[98]
Raytheon	Coyote	Tandem	Canister	1 propeller	Electric	[5,56,100]
Textron	Battlehawk	Conventional	Canister	1 propeller	Electric	[4,5,101,102]
Uvision	Hero-20	Cruciform	Canister	1 propeller	Electric	[74,103,104]
Uvision	Hero-30	Cruciform	Canister	1 propeller	Electric	[2,4,73,74,103–106]
Uvision	Hero-70	Cruciform	Canister	1 propeller	Electric	[4,74,103,107]
Uvision	Hero-120	Cruciform	Canister	1 propeller	Electric	[2,4,74,103,108]
Uvision	Hero-120NG	Cruciform	Canister	1 propeller	Electric	[103]
Uvision	Hero-250	Conventional	Launcher/ canister	1 propeller	Piston	[74,103]
Uvision	Hero-400	Conventional	Launcher/ canister	1 propeller	Piston	[4,74,103,109]
Uvision	Hero-400EC	Cruciform	Launcher/ canister	1 propeller	Electric	[2,74,103,104]
Uvision	Hero-900	Conventional	Launcher/ canister	1 propeller	Piston	[74,103]
Uvision	Hero-1250	Conventional		1 propeller	Piston	[74]
Yemen						
Unknown	Samad-2	Conventional	Launcher	1 propeller	Piston	[45]
Unknown	Samad-3	Conventional	Launcher	1 propeller	Piston	[45]

*The Qasef-2K is an upgrade of the Qasef-1. The exact differences between the two models are unclear.

Table B2
Loitering weapon systems performance, weights and dimensions.

Manufacturer	Name	MTOM/ kg	$m_{warhead}$/ kg	Endurance/ min	Comm. Range/km	Wing span/m	Wing area/m^2	Length/ m	Aspect ratio [–]	Ref.
Armenia										
ProMAQ	Hreesh	7			20					[55]
Australia										
Defendtex	Drone-40			20	10					[26]
Belarus										
Scientific-Manufacturing Centre of Multipurpose Unmanned Systems	Burevestnik MB		10	40						[24,25]
China										
China Aerospace Science and Technology Corporation	CH-901	9.1	2.7	120	15			1.2		[56–58]
Europe										
MDBA Missile Systems	Fire Shadow	200	22	360	140	4.8*	1.9*	4.0	11.9	[4,5,59,60]
Indonesia										
PT Enrol Sistem	Enrol Pilot	3	0.8	20	40	1.2	0.33*	0.8	4.4	[61]
Iran										
Iran Aircraft Manufacturing Industrial Company (HESA)	Qasef-1/Ababil-2t	85	30	120	100	3.0	1.35	2.5	6.7*	[56,62–65]
Iran Aircraft Manufacturing Industrial Company (HESA)	Qasef-2K									[3,65]
Israel										
Aeronautics	Orbiter 1 K	11	2.6	150	100	2.2**	0.87*	1.41	5.6*,**	[2,66–68]
Elbit Systems	Sky Striker		5–10	60–120	40					[69,70]
IAI	Green Dragon	15	3	150	40	1.7	0.28*	1.6	10.3*	[2,71,72]
IAI	Harop		23	360	150	3.0	3.1*	2.5	2.9*	[2,5,56,73,74]
IAI	Harpy	135	32	120		1.3*	0.97*,**	2.1	1.8*	[5,74–77]
IAI	Harpy NG	160	16	540	200	2.6*	1.31*	2.1	5.1*	[4,5,74,76,78]
IAI	Mini Harpy	40	8	120	100	2.9	0.96*	2.5	8.8*	[79]
IAI	Rotem	5.8	1.2	45	10					[2,71]
Rafael Advanced Defence Systems	Spike Firefly	3	0.35	15	1					[80]
Poland										
WB Electronics	Warmate	5.3	1.4	70	12	1.6	0.35*	1.1	7.3*	[4,67,81,82]
WB Electronics	Warmate 2	30	3	120	20					[83]
WB Electronics	Warmate TL					1.7		1.1		[83]
WB Electronics	Warmate V	7		30	12					[84]
Russia										
Zala Aero Group	KYB-UAV	19***	3	30		1.2	0.52*	0.95	2.8*	[85,86]
Zala Aero Group	Lantset 1	5	1	30	40					[86]
Zala Aero Group	Lantset 3	12	3	40	40					[86]
South Korea										
Korean Aerospace Industries	Devil Killer	25	2	10		1.3	0.47*	1.5	3.6*	[5,87–89]
Turkey										
STM	Alpagu	1.9		10	5				6.1*	[90]
STM	Kargu	6.3	1.4	15	5					[90]
STM	Kargu-2	6.8	1.4	30	9.6					[91]
Ukraine										
CDET	RAM	8–10	2–4	60–30		0.23				[92]
United States										
AeroVironment	Switchblade 300	2.5	0.3	20	10	0.69	0.05	0.5	9.5	[4,93,94]
AeroVironment	Switchblade 600	22.7	1.5	40	40	1.8*	0.37*	1.3	9*	[93–95]
Boeing	Persistent Munition Technology Demonstrator	27				3.7		0.8		[5,96]
L3 Technologies	Cutlass	6.8	1.4	60	56	1.4		0.8		[5,97]
Lockheed Martin Missiles and Fire Control	Terminator	2.7	0.4	30	5					[4,98,99]
Lockheed Martin Missiles and Fire Control	Terminator (new version)									[98]
Raytheon	Coyote	5.9	0.9	60		1.5	0.23*	0.9	9.6*	[5,56,100]
Textron	Battlehawk	2.4	0.4	30	5	0.86	0.14*	0.45	5.3*	[4,5,101,102]
Uvision	Hero-20	1.8	0.2	20	10	0.56	0.05	0.64	5.8	[74,103,104]
Uvision	Hero-30	3	0.5	30	40	0.7	0.08	0.8	5.8	[2,4,73,74,103–106]
Uvision	Hero-70	7	1.2	45	40	0.8	0.11	1	5.8	[4,74,103,107]
Uvision	Hero-120	12.5	3.5	60	40	1.5	0.30	1.34	7.5	[4,74,103,104,108],
Uvision	Hero-120NG	12.5	4.5	60	40					[103]
Uvision	Hero-250	25	5	180	150	2.4	0.43	1.8	13.4	[74,103]
Uvision	Hero-400	25	8	240	150	3	0.64	2.2	14.1	[4,74,103,109]
Uvision	Hero-400EC	40	10	120	150	2.4	0.70	2.1	8.2	[74,103,104]

(*continued on next page*)

Table B2 (*continued*)

Manufacturer	Name	MTOM/ kg	$m_{warhead}$/ kg	Endurance/ min	Comm. Range/km	Wing span/m	Wing area/m^2	Length/ m	Aspect ratio [–]	Ref.
Uvision	Hero-900	97	20	420	250	3.6	0.86	2.5	15	[74,103]
Uvision	Hero-1250	125	30		200					[74]
Yemen										
Unknown	Samad-2	87.5	18	402		4.5	1.44	2.8	14.1	[45]
Unknown	Samad-3	107.4	18	808		4.5	1.44	2.8	14.1	[45]

*Dimension based on analysis of pictures in public domain.
**Wing span excluding winglets.
***Weight estimated on reported minimum airspeed, estimated wing area and estimated maximum lift coefficient.

References

[1] Detsch J. The U.S. Army goes to school on nagorno-karabakh conflict. Foreign police. 2021 March 30.
[2] Egozie A. The first loitering weapon systems war. Israel Homeland Security; 2020. https://i-hls.com/.
[3] Gunaratne DR, Himmiche A, Thompson H. Tougas M paes W. Final report of the Panel of Experts on Yemen. United Nations Security Council; 2020 April. Report No.: S/2020/326.
[4] Hughes R. Loitering with intent. Jane's international defence review. 2015 Nov 27.
[5] Gettinger D, Holland MA. Loitering munitions in focus. The Center for the Study of the Drone at Bard College; 2017.
[6] Li Z, Li X. Design and analysis of active disturbance rejection attitude controller for loitering munition. In: Proceedings - 2016 8th international conference on intelligent human-machine systems and cybernetics, IHMSC 2016; 2016 Dec 14. p. 472–5. Zhejiang, China.
[7] Li ZY, Li XM, Liu QS. Trajectory tracking algorithm for motion compensation of loitering munition under wind environment. Binggong Xuebao/Acta Armamentarii 2016 Dec;37(12):2377–84.
[8] Guo MF, Fan NJ, Yuan ZH. Battlefield operational strategy of loitering munition. Binggong Xuebao/Acta Armamentarii. 2006 Sep;27(5):944–7.
[9] Wang Z, Wang H. Target location of loitering munitions based on image matching. In: Proceedings of the 2011 6th IEEE conference on industrial electronics and applications, ICIEA 2011; 2011 June 21-23. p. 606–9. Beijing China.
[10] Wang Z, Wang H, Han J. High accuracy ground target location using loitering munitions platforms. In: Proceedings of SPIE - the international society for optical engineering; 2011 May 24 [Beijing, China].
[11] Wang S, Shi D, Dong Y, Huang K. Research on distributed task allocation of loitering munition swarm. In: Proceedings - 2020 international conference on information science, parallel and distributed systems, ISPDS 2020; 2020 Oct 20-22. p. 162–6. Vienna, Austria.
[12] Liu S, Fan NJ, Yang Z. Fuze warhead coordination design of loitering munitions in view of hit point, vol. 30. Beijing Ligong Daxue Xuebao/Transaction of Beijing Institute of Technology; 2010 Sep. p. 1013–6. 9.
[13] He GL, Ji XL, Zhang TH. Numerical simulation research of loitering munitions aerodynamics. J Beijing Inst Technol (Soc Sci Ed) 2009 Sep;18(3):258–61.
[14] Ji XL, He GL. Aerodynamic characteristics of gun-launched loitering munitions and its shape design, vol. 28. Beijing Ligong Daxue Xuebao/Transaction of Beijing Institute of Technology; 2008 Nov953–956+961. 11.
[15] Wu C, Yuan X, Xue J, Che X, Wang G, Li S. Design and test verification of small loitering munition electric-powered propulsion system. Hangkong Dongli Xuebao/J. Aerospace Power. 2021 Jan;36(1):88–96.
[16] Hao F, Chang M, Tang S. Comparative analysis on primary parameters of loitering munitions of different propulsion systems. Beijing Hangkong Hangtian Daxue Xuebao/J. Beijing Univ. Aeronaut. Astronaut. 2016 Aug;42(8):1612–8.
[17] Cook MV. Flight dynamics principles. A linear systems approach to aircraft stability and control. second ed. Burlington: Elsevier Engineering Series; 2007.
[18] Pinsker WJG. The control characteristics of aircraft employing direct-lift control. Royal Aircraft Establishment Aerodynamics Department; 1968. Reports and Memoranda 3629.
[19] McNeill WE, Gerdes R, Innis RC, Ratcliff JD. A flight study of the use of direct-lift-control flaps to improve station keeping during in-flight refueling. NASA Technical Memorandum; 1973 Oct. Report No.: NASA-TM-X-2936.
[20] Galffy A, Böck M, Kugi A. Nonlinear 3D path following control of a fixed-wing aircraft based on acceleration control. Contr Eng Pract 2019 May;86:56–69.
[21] Nickel K, Wohlfahrt M. Tailless aircraft in theory and practice. American Institute of Aeronautics and Astronautics (AIAA Education Series); 1994.
[22] Stenfelt G, Ringertz U. Yaw control of a tailless aircraft configuration. J Aircraft 2010 September-October:1807–10.
[23] Atherton K. Lightweight loitering munition promises to be as accurate as the human piloting it. C4ISRNET. 2017, June 8.
[24] Novichok N. Belarus unveils new UAVs and UCAVs. Jane's International Defence Review. 2018 July 6.
[25] Local-made Burevestnik-MB armed drone in service with Belarus army. Army recognition. 2018 July 10.
[26] Available from: Soldier systems. An industry daily website [Internet] SOFIC 19 – DefendTex Drone-40. 16 April 2021. https://soldiersystems.net/2019/05/24/sofic-19-defendtex-drone-40/.
[27] Torenbeek E. Synthesis of subsonic airplane design. Rotterdam: Nijgh-Wolters-Noordhoff Universitaire Uitgevers B.V.; 1976. p. 146.
[28] Raymer DP. Aircraft design: a conceptual approach. Washington, D.C.: American Institute for Aeronautics and Astronautics Education Series; 1992. p. 395–409.
[29] Verstraete D, Palmer JL, Hornung M. Preliminary sizing correlations for fixed-wing unmanned aerial vehicle characteristics. J Aircraft 2018;55(2):715–26. 2018.
[30] Oktay T, Uzun M, Ozdemir Kanat O. Maximum lift/drag ratio improvement of TUAVs via small aerodynamic modifications. Aircraft Eng Aero Technol 2018;90(9):1438–44.
[31] Oktay T, Çoban S. Simultaneous longitudinal and lateral flight control system design for both passive and active morphing TUAVs. Elektron. Elektrotech. 2017;23(5):15–20.
[32] Rogoway T. Meet Israel's 'suicide squad' of self-sacrificing drones. The Drive 2016 Aug 8.
[33] Gunaratne DR, Baly MS, Thompson H, Tougas M, Paes W. Final report of the Panel of Experts on Yemen. United Nations Security Council; 2021 Jan. Report No.: S/2021/79.
[34] Drag of circular cylinders normal to a flat plate with turbulent boundary layer for Mach numbers up to 3. Engineering sciences data unit (ESDU). 1983 Aug. Data Item 83025.
[35] Williams JE, Vukelich SR. The USAF stability and control digital DATCOM. Volume I. User's manual. Air Force Flight Dynamics Laboratory (AFFDL); 1979 Nov. AFFDL-TR-79-3032 Volume I.
[36] Torenbeek E. Synthesis of subsonic airplane design. Rotterdam: Nijgh-Wolters-Noordhoff Universitaire Uitgevers B.V.; 1976. p. 487–519.
[37] Shevell RS. Fundamentals of flight. second ed. Pearson; 1989.
[38] Raymer DP. Aircraft design: a conceptual approach. Washington, D.C.: American Institute for Aeronautics and Astronautics Education Series; 1992. p. 280–97.
[39] Hoerner SF. Fluid-Dynamic Drag. Theoretical, Experimental and Statistical Information. Hoerner Fluid Dynamics. 1965. 6. 6-6–17.
[40] Drela M, Youngren H. Athena vortex lattice [internet]. 2020 May 22. Available from: http://web.mit.edu/drela/Public/web/avl/.
[41] Approximate parametric method for propeller thrust estimation. Engineering Sciences Data Unit (ESDU); 1983 Nov. Data Item 83001.
[42] Approximate Parametric Method for Propeller Thrust Estimation. Addendum A: application to fixed-pitch propellers. Engineering Sciences Data Unit (ESDU); 1983 Nov. Data Item 83028.
[43] Verstraete D, MacNeill R. The effects of blockage on the performance of small propellers. In: 20th australasian fluid mechanics conference; 2016 December 5-8 [Perth, Australia].
[44] Ruijgrok GJJ. Elements of airplane performance. second ed. Delft: VSSD; 2009.
[45] Voskuijl M, Dekkers TM, Savelsberg R. Flight performance analysis of the Samad attack drones operated by Houthi armed forces. J. Sci. Glob. Sec. 2020 Dec 10;28(3):113–34.
[46] Oktay T, Eraslan Y. Computational fluid dynamics (CFD) investigation of a quadrotor UAV propeller. In: Proceedings of ICEESEN2020; 2020 June 5-7 [Kayseri, Turkey].
[47] The ventusky web application [Internet]. [cited 22 April 2021] Available from: www.ventusky.com.
[48] Inbar T. Rare -almost intact - example of Houthi (Iranian made) attack drone found Marib in Yemen. This is the mysterious delta winged UAV that was used to attack Saudi infrastructure in. 2019 [Internet] Twitter 2020 Sep 26. Available from: https://twitter.com/inbarspace/status/1309813738195873792.
[49] Lamar JE, Herbert HE. Production version of the extended NASA-langley vortex lattice FORTRAN computer program – volume I – user's guide. NASA; 1982 Apr. Technical Memorandum TM-83303.
[50] Lamar JE, Herbert HE. Production version of the extended NASA-langley vortex lattice FORTRAN computer program – volume II – source code. NASA; 1982 Apr. Technical Memorandum TM-83304.
[51] Margason RJ, Lamar JE. Vortex lattice FORTRAN program for estimating subsonic aerodynamic characteristics of complex planforms. NASA; 1971

Feb. Technical Note D-6142.
[52] Lamar JE, Gloss BB. Subsonic aerodynamic characteristics of interacting lifting surfaces with separated flow around sharp edges predicted by a vortex-lattice method. NASA; 1975 Sep. Technical Note D-7921.
[53] Torenbeek E. Advanced aircraft design. Conceptual design, analysis and optimization of subsonic civil airplanes. Chisester. John Wiley and Sons, Ltd; 2013.
[54] Hoblit FM. Gust loads on aircraft: concepts and applications. first ed. Washington, D. C.: AIAA Education Series; 1988.
[55] Dombe AR. Armenia displays new loitering munitions; one resembling UVision's hero-30. Israel Defence; 2020 April 2.
[56] Military Factory [Internet]. Loitering munition UAVs. 16 April 2021. Available from: https://www.militaryfactory.com/aircraft/loitering-munition-uavs.asp.
[57] China defense industry presents CH-901 suicide drone at SOFEX 2018. Army recognition. 2018 May 9.
[58] Trevithick J. China conducts test of massive suicide drone swarm launched from A box on A truck. The Drive 2020 Oct 14.
[59] Pengeley R. Fire Shadow targets early operational capability. Jane's Int. Def. Rev. 2009.
[60] Scott R. Fire Shadow Loitering Munition project passes first firing mark. Jane's International Defence Review; 2008.
[61] Adjie Haryo. Enrol pilot – inilah drone khusus kamikaze pertama rancangan Indonesia. Indomiliter 2020, Dec 3 [Indonesian].
[62] Himmiche A, Carvajal FR, Gunaratne DR, Johnsen G, Wilkinson A. Final report of the Panel of Experts on Yemen. United Nations Security Council; 2018 Jan. Report No.: S/2018/68.
[63] Himmiche A, Carvajal FR, Paes W, Thompson H, Tougas M. Final report of the Panel of Experts on Yemen. United Nations Security Council; 2019 Jan. Report No.: S/2019/83.
[64] Binnie J. Yemeni rebels display UAVs. Jane's Defence Weekly; 2017.
[65] Houthi suicide drones strike Saudi King Khalid Airbase. Defence point.com. 2019 July 25.
[66] Williams H. Paris Air Show 2015: aeronautics draws on UAV technology for new loitering munition. Jane's International Defence Review; 2015.
[67] Gettinger D. The drone databook. The Center for the study of the Drone at Bard College; 2019.
[68] Aeronautics Group. Orbiter® 1K Loitering Munition UAS. Available from: https://aeronautics-sys.com/wp-content/themes/aeronautics/pdf/orbiter_1k_v2.pdf.
[69] Valpolini P. New strike and surveillance systems from Elbit Systems. European Defence Review; 2019.
[70] Elbit Systems [Internet] Skystriker. Available from: https://elbitsystems.com/product/skystriker/; 16 April 2021.
[71] Valpolini P. New loitering munitions from IAI. European Defence Review; 2018.
[72] Israel Aerospace Industries (IAI). Green DragonTM compact tactical loitering munition. 2019. Available from: https://www.iai.co.il/p/green-dragon.
[73] Egozie A. The big leap forward for loitering weapons. Israel Homeland Security; 2020. Available from: https://i-hls.com/archives/65896.
[74] Boulanin V, Verbruggen M. Mapping the development of autonomy in weapon systems. Stockholm International Peace Research Institute (SIPRI); 2017 Nov.
[75] Harpy heralds new customers. Jane's international defence review. 1997.
[76] Harpy air defense suppression system. Defense update. 2006.
[77] Turbosquid 3D Models for Professionals [Internet] 3D model IAI Harpy Loitering Munition by ES3DStudios. Available from: https://www.turbosquid.com/FullPreview/Index.cfm/ID/1436173; 16 April 2021.
[78] Israel Aerospace Industries (IAI). Harpy anti radiation loitering weapon system. 2019. Available from: https://www.iai.co.il/p/harpy.
[79] Israel Aerospace Industries (IAI). Mini Harpy multi-purpose tactical loitering munition. 2019. Available from: https://www.iai.co.il/p/mini-harpy.
[80] Rafael Advanced Defence Systems Ltd. SPIKE FIREFLYTM miniature tactical loitering weapon behind-cover precision attack capabilities for the dismounted soldier. 2017.
[81] WB Group [Internet]. Warmate loitering munitions. 21 April 2021. Available from: https://www.wbgroup.pl/en/produkt/warmate-loitering-munnitions/.
[82] Remigiusz R. WB Group to launch SWARM system. Jane's Int. Def. Rev. 2017.
[83] Kutnik S. Warmate 2. The only circulating ammunition system in Europe … from Poland. Aviat. Int. 2018;9:14–5.
[84] MSPO. WB Group unveils its WARMATE V quadcopter VTOL loitering munition system. Army Recognition; 2019. p. 2019.
[85] Russia's Kalashnikov Unveils KYB-UAV Suicide Drone at IDEX 2019. DefPost, A comprehensive Aerospace and defence portal. 2019.
[86] Zala Aero Group [Internet]. Unmanned aerial vehicle. 21 April 2021. Available from: https://zala-aero.com/en/production/bvs/.
[87] Brown N. Idex 2013: KAI shows off 'loitering' precision munition. Jane's International Defence Review; 2013.
[88] Miller D. South Korea developing kamikaze-style drone that dive bombs the enemy at 250 mph. Daily Mail; 2012.
[89] Korea Aerospace Industries, Ltd. (KAI) [Internet]. Unmanned aerial vehicles. 21 April 2021. Available from: https://www.koreaaero.com/EN/Business/UAV.aspx.
[90] Available from: STM. [Internet] unmanned systems. 21 April 2021. https://www.stm.com.tr/en/our-solutions/autonomous-systems.
[91] Hambling D. Turkish military to receive 500 swarming kamikaze drones. Forbes; 2020.
[92] Novichkov N. Ukraine unveils new RAM loitering munition. Jane's Defence News; 2020 March 9.
[93] Reim G. AeroVironment unveils anti-armour Switchblade 600 loitering munition. Flight Glob. 2020.
[94] AeroVironment [Internet]. Tactical missile systems. 16 April 2021. Available from: https://www.avinc.com/tms.
[95] Valpolini P. Switchblade 600, the new medium range loitering munition. European Defence Review; 2020.
[96] Boeing persistent munition technology demonstrator achieves autonomous flight. Aerotech News 2006;21(26).
[97] Russian Unmanned Vehicle Systems [Internet] Cutlass. Available from: https://en.ruvsa.com/catalog/cutlass/; 16 April 2021.
[98] Drew J. Lockheed displays new-look Terminator UAV. Flight Global; 2015.
[99] Williams H. Auvsi 2013: terminator targets LMAMS requirement. Jane's Int. Def. Rev. 2013 Aug 14.
[100] Raytheon Missiles and Defence [Internet]. Coyote UAS. 16 April 2021. Available from: https://www.raytheonmissilesanddefense.com/capabilities/products/coyote.
[101] Steadman B, Finklea J, Kershaw J, Loughman C, Shaffner P, Frost D, Deller S. Advanced micro observer UGS integration with and cueing of the Battlehawk squad level loitering munition and UAV. In: Proceedings of SPIE 9079, ground/air multisensor interoperability, integration, and networking for persistent ISR V, 90790D; 2014 June 10. https://doi.org/10.1117/12.2049645. Amsterdam, The Netherlands.
[102] Williams H. Auvsi 2013: textron Leverages loitering munition technology for new ISR UAV. Jane's Int. Def. Rev. 2013 Aug 16.
[103] Hughes R. New vision: Israel's loitering weapon system house opens its doors. Jane's International Defence Review. 2020 May 4.
[104] Eshel T. UVision introduces new multi-mission loitering weapons. Defence-update; 2019 June 20.
[105] Avia.pro [Internet]. Uvision 30 Hero. 16 April 2021. Available from: https://avia-pro.net/blog/uvision-hero-30-tehnicheskie-harakteristiki-foto.
[106] Lappin Y. IDF using UVision mini loitering munition. Jane's. 2020 July 16.
[107] Avia.pro [Internet]. Uvision 70 Hero. 16 April 2021. Available from: https://avia-pro.net/blog/uvision-hero-70-tehnicheskie-harakteristiki-foto.
[108] Avia.pro [Internet]. Uvision 120 Hero. 16 April 2021. Available from: https://avia-pro.net/blog/uvision-hero-120-tehnicheskie-harakteristiki-foto.
[109] Avia.pro news website: https://avia-pro.net/blog/uvision-hero-400-tehnicheskie-harakteristiki-foto [accessed 29-12-2020].